Procrystalline Self-Assembly of Desymmetrized Pentaphenylcyclopentadiene

Donglin Li, Sota Seki, Atsushi Ishikawa, Kenichiro Omoto, Kazuma Yasuhara, Gwénaël Rapenne, Shigeki Kawai

Procrystalline Self-Assembly of Desymmetrized Pentaphenylcyclopentadiene

Donglin Li,[‡1] Sota Seki,[‡2] Atsushi Ishikawa,*[3] Kenichiro Omoto,[§2] Kazuma Yasuhara,[2,4] Gwénaël Rapenne*[2,5] and Shigeki Kawai*[1,6]

[1]Center for Basic Research on Materials, National Institute for Materials Science, 1-2-1, Sengen, Tsukuba, Ibaraki 305-0047, Japan.
[2]Division of Materials Science, Nara Institute of Science and Technology, 8916-5 Takayama, Ikoma, 630-0192, Japan.
[3]Department of Transdisciplinary Science and Engineering, School of Environment and Society, Tokyo Institute of Technology, 2-12-1 Ookayama, Meguro-ku, Tokyo, 152-8552, Japan
[4]Center for Digital Green-innovation, Nara Institute of Science and Technology, 8916-5 Takayama, Ikoma, Nara, 630-0192, Japan.
[5]CEMES, Université de Toulouse, CNRS, 29, rue Marvig, 31055 Toulouse, France
[6]Graduate School of Pure and Applied Sciences, University of Tsukuba, Tsukuba 305-8571, Japan.
‡ These authors contributed equally.
§ Current address: Division of Chemistry and Materials Science, Graduate School of Integrated Science and Technology, Nagasaki University, 1-14, Bunkyo-machi, Nagasaki, 852-8521, Japan.

E-mail: ishikawa.a.ai@m.titech.ac.jp, gwenael-rapenne@ms.naist.jp,

KAWAI.Shigeki@nims.go.jp

Abstract

The interplay between the molecular shape and the intermolecular interaction plays a decisive role in self-assembled structures. Recently, inherent randomness of low ordered assemblies, resulting from lack of short- and long-range periodicities, has attracted significant attention due to the unique structural, electronic, and mechanical properties. Here, we present procrystalline self-assemblies of pentaphenyl cyclopentadienyl derivatives on Ag(111) and Au(111) with scanning tunneling microscopy, operating at 4.3 K under ultra-high vacuum conditions. Two

examples, using five-fold symmetric molecules substituted with methyl or fluorine groups, show that weak interactions, such as π-π stacking, CH-π interactions, and CH···F hydrogen bonding, play a pivotal role in formation of the procrystalline assembly. Our results may give insights into the intricate relationship between the molecular shape and the intermolecular interaction in the formation of non-crystalline assemblies.

Keywords: Scanning tunneling microscopy, cyclopentadienyl derivatives, procrystalline, self-assembly, five-fold symmetric molecules

Introduction

Self-assembly stands as an important phenomenon in chemistry and materials science,[1] where molecules as building blocks spontaneously arrange themselves into ordered structures by non-covalent interactions, such as dipole-dipole interaction,[2] hydrogen bonding,[3-5] van der Waals forces,[6] and π-π stacking.[7,8] Scanning Tunneling Microscopy (STM) is a powerful technique to visualize self-assembled structures with exceptional resolution, down to the atomic scale. By scanning the tip on surface while controlling the tip-sample distance with a given tunneling current between a sharp metal tip and a sample, individual atoms and molecules on surface are routinely resolved in STM topographies. This capability also facilitates direct observation and characterization of self-assembled monolayers, metal organic frameworks, and covalent organic frameworks.[9-14] A number of studies on self-assemblies with STM have resulted in important discoveries, which elucidate the fundamental principles governing molecular organization at the nanoscale. Researchers, leveraging this approach to explore the dynamics of self-assembly processes, have investigated the influence of external factors,[15-17] and engineered complex nanostructures with tailored properties and functionalities in different environments.[18-20]

Contemporary research in molecular self-assembly is predominantly focused on the design and fabrication of crystalline materials, driven by the short- and long-range periodicities as well as crystal symmetry. The characteristics govern a diverse array of correlated properties, including electronic states, magnetic order, piezoelectricity, and ferroelasticity.[21-23] Recent attention has also been drawn towards disordered states, which possess the potential to exhibit advanced functionalities arising from inherent randomness.[24,25] Quasi-crystals represent a captivating class of non-crystalline structures characterized by a long-range order but lacking a periodicity of traditional crystals, resulting in distinctive structural properties.[26,27] Assisted by STM, numerous quasi-crystals have been synthesized, shedding light on the growth

mechanisms.[28,29] Similarly, procrystalline structures also constitute a prevalent type of non-crystalline assembly, where building blocks are arranged periodically but with random orientation, indicating the absence of translational periodicity.[30] At the heart of these non-crystalline structures is the design of the building blocks, a critical aspect enabling precise manipulation of symmetry, domain size, and electronic properties during the self-assembly process. For example, pentagon building blocks, with the inherent five-fold symmetry, present an ideal candidate for inducing incompatibility with translational symmetry.[31-33] Therefore, a deep understanding of the intricate relationship between building blocks and procrystalline structures is crucial for advancing our knowledge of materials science and exploiting novel structures for technological applications.

Here, we employ pentaphenyl cyclopentadienyl (Cp) derivatives (Scheme 1) to investigate formation of non-crystalline molecular assemblies with five-fold symmetric building blocks. Methyl and fluoro groups were introduced at the *m*-position to study how the functional groups affect the molecular assemblies on Au(111) and Ag(111) surfaces at low temperature with STM. Both molecules form procrystalline structures, in which each unit is periodically positioned but randomly oriented, underscoring the significance of pentagon building blocks in the non-crystalline assembly process. The weak intermolecular interaction may afford greater freedom, allowing for structural disorder.

Result and discussion

Synthesis of the Cp derivatives

Two meta-substituted Cp were synthesized in two steps from commercially available tetraphenylcyclopentadienone. First, the addition of the *m*-lithiotoluene or the *m*-lithioflurobenzene on the tetraphenylcyclopentadienone gave the corresponding cyclopentadienol which was converted to its brominated analog by reaction with hydrobromic

acid in acetic acid. The methyl and fluoro-functionalized Cp were obtained with an overall yield of 35 % and 32 %, respectively (see Supplementary Information for more details and characterization). The brominated Cp were obtained as a mixture of three regioisomers due to a unimolecular nucleophilic substitution (S_N1) mechanism,[34,35] however, the three regioisomers can be converted into the same radical species during sublimation by cleaving the C-Br bonds (Scheme 1) like it has been shown on a molecule with a common bromocyclopentadiene sub-unit. [36]

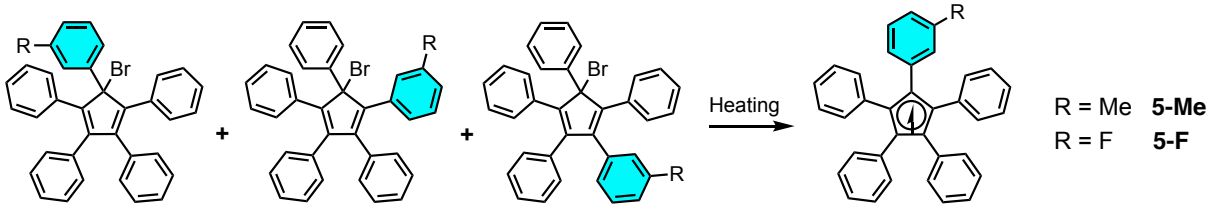

Scheme 1. Chemical structures of Cp derivatives functionalized with R = Me (**5-Me**) and F (**5-F**). The brominated precursor is a mixture of three regioisomers. During sublimation, the debromination takes place and subsequently the radical is stabilized by connecting to the metal substrate.

STM observation of 5-Me

5-Me was deposited on a clean Au(111) surface kept at room temperature (Figure 1a). We found that single molecules adsorbed at the hcp elbow sites as indicated by white arrows and extended molecular islands formed along the fcc sites. Figure 1b shows a close-up view of a single molecule, in which five dots are seen. The apparent highest dot likely corresponds to the methyl-functionalized phenyl group. We extracted the characteristic shape composed of one large and two small dots as described in Figure 1c for analysis of the self-assembly. Figure 1d shows the calculated structure of a single **5-Me** on Au(111), where the methyl-functionalized phenyl group is in a tilted configuration. The adjacent two non-functionalized phenyl groups lie flat on the surface, while the remaining two phenyl groups are also tilted. At the fcc site,

several triangular shaped structures were observed. The characterization of the simulated STM image (Figure S1a) based on the optimized structure shows good agreement with the experimental results. To investigate the self-assembly, a close-up view of the STM topography was taken (Figure 1e). We found that the structure was composed of three molecules with the methyl functionalized phenyl groups positioned at the corners of the triangular cluster. Similar to a single molecule adsorbed at the elbow site, two dots were observed among the ternary molecules, attributed to the tilting phenyl groups. For clarity in analyzing the self-assembled structure, the molecules are labeled as I-III. By superimposing the optimized structural model of **5-Me** onto the STM image of this trimer (Figure S2a), it was identified that Molecule I and Molecule III are condensed via π-π stacking, while CH-π interactions exist between Molecule I and Molecule II, as well as between Molecule II and Molecule III. These two types of interactions induce the asymmetric self-assembled structure. Conversely, the symmetrical trimer is formed by three sets of π-π stacking between the units (Figure S2b), resulting in a chiral structure (Figure 1f). Another trimer with a different chirality was also observed (Figure S3). In addition to the three-molecule clusters, tetramer clusters were found, with methyl-substituted phenyl groups positioned at each corner of the rhombus. The positions of the tilting phenyl groups in the tetramer are consistent with those in the asymmetric trimer. The superimposed structural model (Figure S2c) indicates that an additional **5-Me**, marked by an arrow in Figure 1g, contacts the edge of the trimer via CH-π interactions. Figures 1h-j provide the schematic illustration of these three structures, which are fundamental components of the extended self-assembled molecular island. Upon analyzing the close-packed self-assembled island (Figure 1k), it was determined that the molecular island comprises trimer and tetramer clusters, denoted by red and green triangles and blue rhombuses, respectively. Despite the condensation of molecules, no regular structure was observed, as shown in the FFT image (inset of Figure 1k). Several molecules displayed a star-shaped conformation, indicated by black

circles. The corrugation amplitude of these star-shaped molecules was smaller than that of the basic three molecular clusters, suggesting that all five phenyl groups of the star-shaped molecule lie on the surface with the same tilt angle. No periodic adsorption of the planar molecules was observed. The low order of the molecular film is attributed to the presence of different adsorption geometries of molecules, resulting from the relatively weak van der Waals interactions between the methyl functionalized phenyl groups. Therefore, this structure can be regarded as long-range disordered and short-range ordered self-assembly. Notably, the formation of the molecular film extended the area of the fcc site, where the herringbone reconstruction was absent (Figure S4). We deduce that the chemical bonds of the Cp to the substrate gold atoms were responsible for the modulation of the herringbone structure.[37] At the same time, since the intermolecular interaction is relatively weak, the corrugated herringbone reconstruction also prevents the extension of the self-assembled structure.

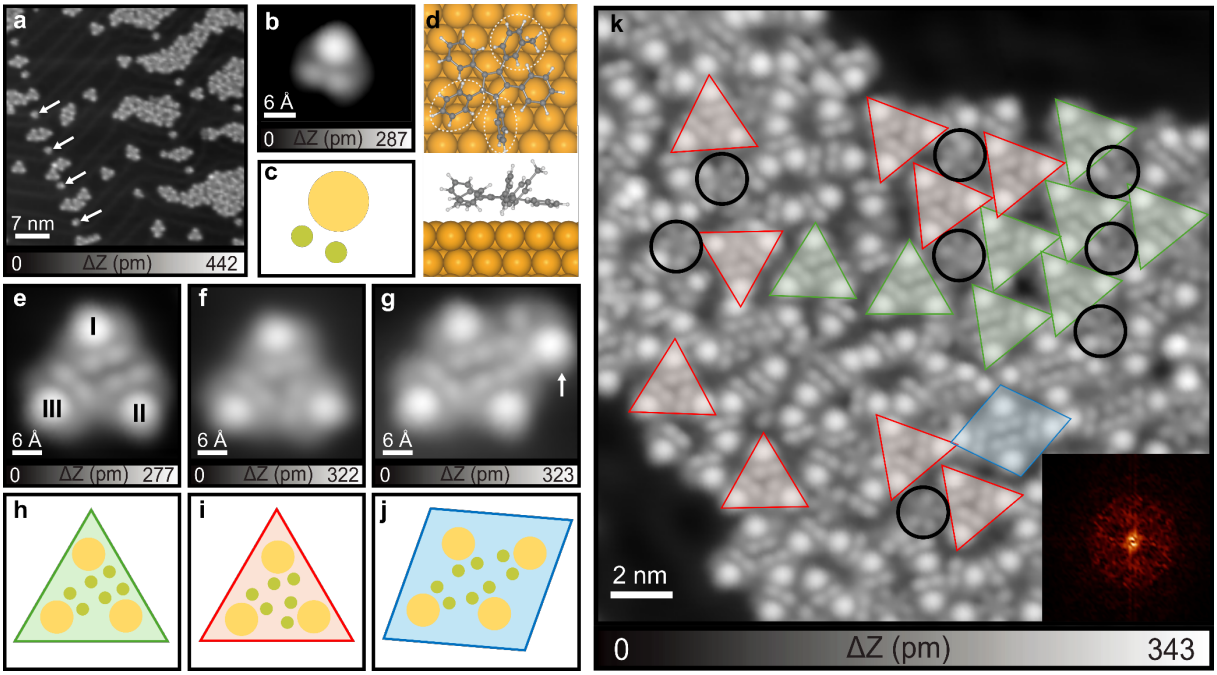

Figure 1. **Self-assembled structures of 5-Me on the Au(111) surface.** (**a**) Large-scale STM topography of the self-assembled structure of **5-Me**. (**b**) Close-up view of the monomer and (**c**) the corresponding schematic illustration of the characteristic shape. (**d**) Optimized structure of 5-Me on Au(111) with the DFT. The carbon, hydrogen, and gold atoms are represented by gray,

white, and yellow spheres, respectively. (**e**-**g**) Close-up views of the asymmetric trimer, symmetric trimer, and tetramer, respectively. (**h**-**j**) Corresponding schematic illustrations of the asymmetric trimer, symmetric trimer, and tetramer, respectively. (**k**) Close-packed molecular island. Green and red triangle represent asymmetric and symmetric trimers, and circles represent monomers, and blue rhombuses represent tetramers. Inset shows the 2D-FFT image of the close-packed structure. Scanning parameter: V = 0.2 V and I = 10 pA.

In order to obtain an extended self-assembly, we deposited **5-Me** molecules on a clean Ag(111) surface (Figure 2a). We found a large molecular island on the surface (Figure S5). The corresponding FFT image shows distinct spots, which arose from the square lattice observed in the STM topography. The formation of the square lattice may be induced by the close packing of rhombus clusters, facilitated by the relatively weak interaction between each unit. To visualize the pore sites, we conducted image thresholding of Figure 2a with the threshold of Z = 52 pm and subsequently reversed the contrast. The square periodicity became more evident in the corresponding image thresholding (Figure 2b). In contrast, the spots in the 2D-FFT image relate to only the position of the molecules and so that the orientational correlation of the molecule cannot be analyzed. Upon a closer inspection of the STM image (Figure 2c), it became evident that the orientation of the units is random as indicated by the superimposed schematic illustration of each molecule. This result indicates the presence of a procrystalline structure rather than a crystalline one, in which the units are positioned periodically but undergo orientational randomly.[30]

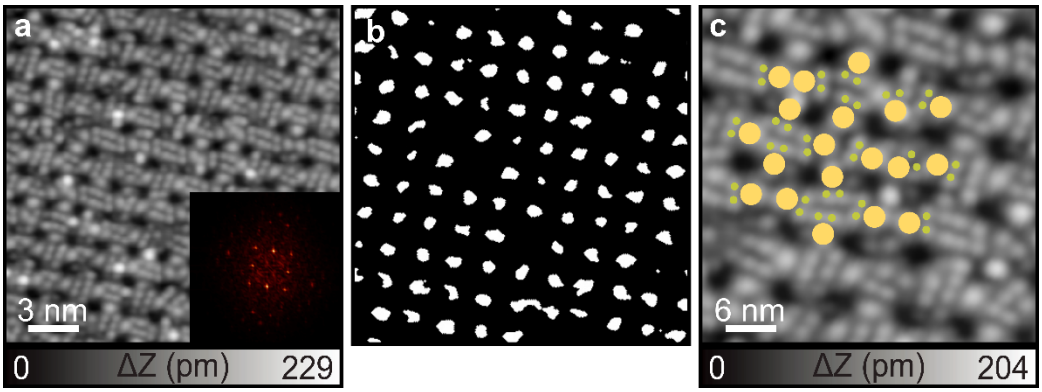

Figure 2. **Self-assembled structure of 5-Me on Ag(111).** (**a**) Large scale STM image of the self-assembled structure of **5-Me**. Inset: Corresponding 2D-FFT image. (**b**) Extracted cavities with thresholding from (a). (**c**) Close-up STM image of the self-assembled structure superimposed with schematic illustration of monomer. Scanning parameter: V = 0.2 V and I = 10 pA.

STM observation of 5-F

Next, we investigated the influence of the strength of intermolecular interaction on the non-crystalline structure. We examined the self-assembly behavior of **5-F**, which could facilitate greater intermolecular interactions through the additional CH···F hydrogen bonding.[38-40] Upon depositing 0.7 monolayer of **5-F** on Au(111) kept at room temperature, we obtained a mixed film consisting of two distinct phases (Figure 3a). In both phases, no significant corrugation, relating to the herringbone structure, was seen. It is obvious that Phase I was composed of star-shaped molecules, while Phase II comprised a mixture of star-shaped and V-shaped molecules. A closer look at the star-shaped molecule shows one bright lobe and four dark lobes, corresponding to the F-functionalized and non-functionalized phenyl groups, respectively (Figure 3b). For a detailed analysis of the film structure, we extracted characteristic shapes of the dominated molecule as showing the star-shaped illustration in Figures 3c. In the V-shaped molecule, only two dark dots appeared alongside one bright dot (F-functionalized

phenyl group). This conformation is similar to that of **5-Me** on the Au(111) surface, where the adjacent two phenyl groups to the F-functionalized phenyl group lie flat on the surface, while the last two are slightly tilted due to steric hindrance. The geometry optimization of **5-F**, performed using DFT and shown in Figure 3d, indicates a flatter geometry compared to **5-Me**. The corresponding simulated STM image (Figure S1b) indicates that the brightest part is related to the F-functionalized phenyl group. This result is consistent with the predominantly flat structure observed in the STM images in Figures 3e and 3f. Closer inspection of Phase I (Figure 3e) reveals long-range orderliness, supported by the periodicity shown in the corresponding 2D-FFT image (inset in Figure 3e). However, similar to the situation observed with **5-Me** on Ag(111), the superposed schematic illustration of molecules in the close-up view STM image shows random orientation, indicating no translational periodicity.[30] Thus, Phase I can also be regarded as the procrystalline structure. Regarding Phase II, the close-up view STM image shows randomness of the positions and the orientation of the star-shaped and V-shaped molecules in the film (Figure 3f). The corresponding 2D-FFT image shows weak six spots in the FFT image, which relates to the three-fold position of the molecule. Thus, Phase II also corresponds to the procrystalline structure. Unlike the self-assembly of **5-Me** on Au(111), **5-F** prefers to self-assemble into island structures, with rare clusters observed (Figure S6). This behavior is attributed to the stronger intermolecular interactions, specifically CH···F hydrogen bonding (Figure S7). We also annealed the film to investigate the potential phase transformation of such spatial molecule.[41] After annealing the film at 100 °C, two new phases were observed, as shown in Figure S8a. Close-up STM images (Figures S8b and S8c) of these phases reveal that both are composed of V-shaped molecules, with no star-shaped molecules present. This indicates that the star-shaped molecules transformed into V-shaped molecules upon annealing. Additionally, the inset FFT demonstrates that phase III exhibits an ordered structure, whereas phase IV is disordered.

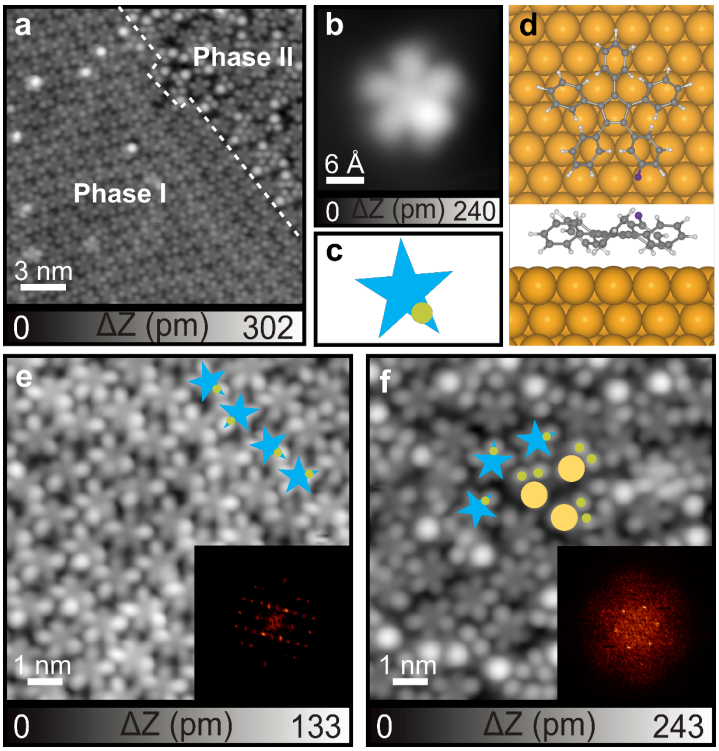

Figure 3. **Self-assembled structure of 5-F on the Au(111) surface displaying two distinct phases.** (**a**) Large scale STM image of the self-assembled structure of **5-F**. (**b**) Close-up view of star-shaped monomers of **5-F** and (**c**) the corresponding schematic illustration. (**d**) The optimized structure of **5-F** on Au(111). The carbon, hydrogen, fluoride and gold atoms are represented by gray, white, purple, and yellow spheres, respectively. (**e,f**) Close-up views of both phases overlaid with schematic illustrations of monomers, revealing the periodic positioning but permuted orientation of phase I and the randomness of phase II. Insets show corresponding 2D-FFT images. Scanning parameter: $V = 0.2$ V and $I = 10$ pA.

To investigate the influence of substrate, we also deposited **5-F** molecules onto Ag(111). In contrast to the case of **5-F** adsorbed on Au(111), only one type of self-assembled structure was formed, exhibiting different chirality (Figures 4a and 4b). The chirality was readily identified by observing the cavity shapes outlined by red and blue contours in Figures 4a and 4b, respectively. The corresponding 2D-FFT image displays bright spots indicative of a six-fold symmetry, suggesting a hexagonal lattice structure for the film—a characteristic of

crystalline structures. Upon closer examination of this film (Figure 4c), the motif was identified as a trimer (red triangles in Figure 4c) which composed of three V-shaped monomers. However, in this case, the V-shaped molecule was composed of two-bright dots and one dark dot instead of one bright dot and two dark dots. This may be attributed to the enhanced interaction between the F atom and the Ag(111) surface, which results in the orientation of the F-functionalized group directed towards the surface. Consequently, the F-functionalized phenyl group appears darker. The superposed schematic illustration of the molecules in Figure 4c reveals translational periodicity in the film structure, thus suggesting a crystalline arrangement in this case. This may result from the stronger intermolecular interactions of CH···F hydrogen bonding between the units on Ag(111).

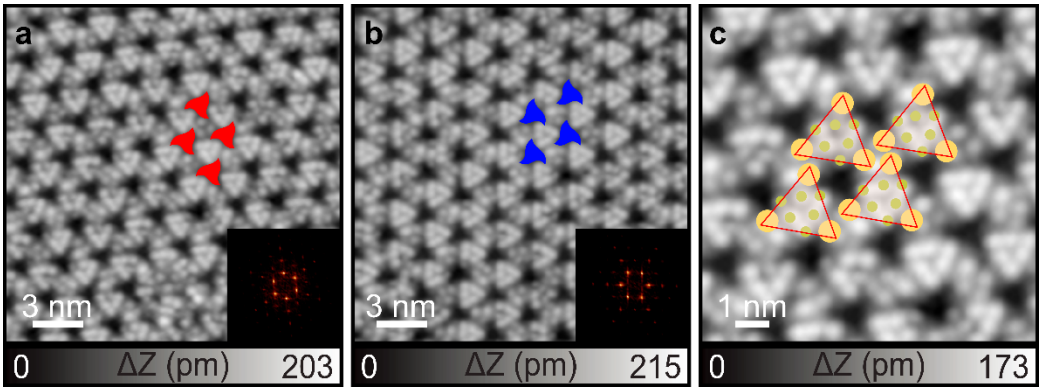

Figure 4. **Self-assembled structure of 5-F on the Ag(111) surface.** (**a**,**b**) Large scale STM images of the self-assembled structure of **5-F** with different chirality, with cavities filled with red and blue contours to indicate their chirality. Insets show the corresponding 2D-FFT image. (**c**) Close-up view STM image of the self-assembled structure superimposed by the schematic illustration of monomer, revealing triangular units. Scanning parameter: V = 0.2 V and I = 10 pA.

Conclusion

In summary, we synthesized two procrystalline structures through rational design of precursor molecules on Au(111) and Ag(111) surfaces. Comparing the distinct behaviors of **5-**

Me and **5-F** on different surfaces, we observed significant influences of both the functional group and substrate on the self-assembly process. Notably, weak interactions such as π-π and CH-π interactions between the building blocks are likely to play a key role in the formation of procrystalline structures, while the stronger interactions such as CH···F hydrogen bonding are more likely to form crystalline structures. These findings offer insights into the intricate relationship between building blocks and non-crystalline assemblies, potentially paving the way for the development of disordered states with advanced functionalities.

Methods

STM experiments: In this work, a homemade low-temperature scanning tunneling microscope (STM) was employed under ultrahigh vacuum conditions ($P < 5\times10^{-10}$ mbar) and a low temperature of 4.3 K. The Au(111) substrate was cleaned through multiple cycles of sputtering with Ar^+ ions and annealing at 700 K for 15 minutes. Temperature monitoring was conducted using a combination of a pyrometer and a thermocouple. The precursors of **5-Me** and **5-F** were synthesized in solution (the details are shown in SI) and subsequently deposited onto the surfaces maintained at room temperature using a standard Knudsen cell (Kentax GmbH). The acquired data were processed using WSxM software.

DFT calculation.

To confirm the experimentally proposed structure of **5-Me** and **5-F**, theoretical calculations with density functional theory (DFT) have been performed. **5-Me** and **5-F** adsorbed on Au(111) surface were modeled with the periodically repeated slabs. The Au surface was constructed from the face-centered cubic Au bulk structure, where an experimental lattice constant of 4.078 Å was used.[42] From this bulk structure, the 8×8×3 supercell was made to form the Au(111)

surface, which contains 256 Au atoms. The bottom two Au layers were fixed during the calculations, while other parts were fully relaxed. Prior to the geometry optimization, the molecular dynamics (MD) calculations were performed to sufficiently explore the configuration space. The MD simulation was done for 1 ps, with 0.5 fs taken as the timestep. The *NVT* ensemble with $T = 100 \pm 10$ K was used, where the Nose-Hoover thermostat was used to control the temperature. After the MD calculation, the geometry optimization was carried out. For the electronic structure calculation, the Gaussian plane wave (GPW) method was used. As the exchange-correlation functional, the Perdew-Burke-Ernzerhof (PBE) plus Grimme's D3 method was used.[43,44] The plane wave energy cutoff was set to 280 Rydberg, and the reciprocal space integration was done with a single **k**-point placed at gamma. To alleviate the artificial interaction between slabs, a vacuum layer of 10 Å thickness was placed between slabs. The thresholds for the electronic structure calculation and geometry optimization were set to 1.0×10^{-5} and 1.0×10^{-4} in energy (Hartree) and force (Hartree/Bohr), respectively. The core electrons were represented by the Gödecker-Teter-Hutter (GTH) pseudopotentials, and the valence electrons were represented by the MOLOPT basis set at double-zeta plus polarization level (DZVP-MOLOPT-SR-GTH).[45] Spin polarization was considered throughout, and the double spin state was used for both **5-Me** and **5-F**. All the calculations were done with CP2K (version 2024.1) software.[46] The visualization was done with the VESTA software.[47] The simulation of STM images were performed by Multiwfn software.[48]

AUTHOR INFORMATION

Corresponding Author

* ishikawa.a.ai@m.titech.ac.jp

* gwenael-rapenne@ms.naist.jp

* KAWAI.Shigeki@nims.go.jp

ACKNOWLEDGEMENTS

This work was supported by the Japan Society for the Promotion of Science (JSPS) KAKENHI Grant-in-Aid for Basic Research A (JP22H00325, JP22H00285, and JP24K21721). The University Paul Sabatier (Toulouse) and NAIST are also warmly thanked for providing a crossed position to G.R.

References

1. Whitesides, G. M.; Grzybowski, B. Self-assembly at all scales. *Science* **2002**, *295*, 2418−2421.
2. Yokoyama, T.; Yokoyama, S.; Kamikado, T.; Okuno, Y.; Mashiko, S. Selective assembly on a surface of supramolecular aggregates with controlled size and shape. *Nature*, **2001**, *413*, 619−621.
3. Hirschberg, J. K.; Brunsveld, L.; Ramzi, A.; Vekemans, J. A.; Sijbesma, R. P.; Meijer, E Helical Self-assembled polymers from cooperative stacking of hydrogen-bonded pairs. *Nature* **2000**, *407*, 167−170.
4. Sherrington, D. C.; Taskinen, K. A. Self-assembly in synthetic macromolecular systems via multiple hydrogen bonding interactions. *Chem. Soc. Rev.* **2001**, *30*, 83−93.
5. Zhang, L.; Long, Y.; Chen, Z.; Wan, M. The effect of hydrogen bonding on self-assembled polyaniline nanostructures. *Adv. Funct. Mater.* **2004**, *14*, 693−698.
6. Gao, H.-Y.; Wagner, H.; Held, P. A.; Du, S.; Gao, H.-J.; Studer, A.; Fuchs, H. In-plane van der Waals interactions of molecular self-assembly monolayer. *Appl. Phys. Lett.* **2015**, *106*, 081606.

7. Claessens, C. G.; Stoddart, J. F. π–π interactions in self-assembly. *J. Phys. Org. Chem.* **1997**, *10*, 254−272.
8. Stöckl, Q.; Hsieh, Y.; Mairena, A.; Wu, Y.; Ernst, K.-H. Aggregation of C_{70}-fragment buckybowls on surfaces: π–H and π–π bonding in bowl up-side-down ensembles. *J. Am. Chem. Soc.* **2016**, *138*, 6111−6114.
9. Adisoejoso, J.; Tahara, K.; Lei, S.; Szabelski, P.; Rzysko, W.; Inukai, K.; Blunt, M. O.; Tobe, Y.; De Feyter, S. One building block, two different nanoporous self-assembled monolayers: A Combined STM and Monte Carlo study. *ACS Nano* **2012**, *6*, 897−903.
10. Barth, J. V.; Weckesser, J.; Trimarchi, G.; Vladimirova, M.; De Vita, A.; Cai, C.; Brune, H.; Günter, P.; Kern, K. Stereochemical effects in supramolecular self-assembly at surfaces: 1-D versus 2-D enantiomorphic ordering for PVBA and PEBA on Ag (111). *J. Am. Chem. Soc.* **2002**, *124*, 7991−8000.
11. Clair, S.; Pons, S.; Seitsonen, A. P.; Brune, H.; Kern, K.; Barth, J. V. STM Study of Terephthalic Acid Self-assembly on Au (111): Hydrogen-bonded sheets on an inhomogeneous substrate. *J. Phys. Chem. B* **2004**, *108*, 14585−14590.
12. Heim, D.; Ecija, D.; Seufert, K.; Auwarter, W.; Aurisicchio, C.; Fabbro, C.; Bonifazi, D.; Barth, J. V. Self-assembly of flexible one-dimensional coordination polymers on metal surfaces. *J. Am. Chem. Soc.* **2010**, *132*, 6783−6790.
13. Otero, R.; Gallego, J. M.; de Parga, A. L. V.; Martín, N.; Miranda, R., Molecular self-assembly at solid surfaces. *Adv. Mater.* **2011**, *23*, 5148−5176.
14. Weigelt, S.; Bombis, C.; Busse, C.; Knudsen, M. M.; Gothelf, K. V.; Lægsgaard, E.; Besenbacher, F.; Linderoth, T. R. Molecular Self-assembly from building blocks synthesized on a surface in ultrahigh vacuum: Kinetic control and topo-chemical reactions. *ACS Nano* **2008**, *2*, 651−660.

15. Elbing, M.; Błaszczyk, A.; von Hänisch, C.; Mayor, M.; Ferri, V.; Grave, C.; Rampi, M. A.; Pace, G.; Samorì, P.; Shaporenko, A. Single component self-assembled monolayers of aromatic azo-biphenyl: influence of the packing tightness on the SAM structure and light-induced molecular movements. *Adv. Funct. Mater.* **2008**, *18*, 2972−2983.
16. Peng, X.; Zhao, F.; Peng, Y.; Li, J.; Zeng, Q. Dynamic Surface-assisted assembly behaviours mediated by external stimuli. *Soft Matter* **2020**, *16*, 54−63.
17. Wan, L.-J. Fabricating and Controlling Molecular Self-organization at solid surfaces: studies by scanning tunneling microscopy. *Acc. Chem. Res.* **2006**, *39*, 334−342.
18. Goronzy, D. P.; Ebrahimi, M.; Rosei, F.; Arramel; Fang, Y.; De Feyter, S.; Tait, S. L.; Wang, C.; Beton, P. H.; Wee, A. T. Supramolecular assemblies on surfaces: Nanopatterning, functionality, and reactivity. *ACS Nano* **2018**, *12*, 7445−7481.
19. Ciesielski, A.; Palma, C. A.; Bonini, M.; Samorì, P. Towards supramolecular engineering of functional nanomaterials: Pre-programming multi-component 2D self-assembly at solid-liquid interfaces. *Adv. Mater.* **2010**, *22*, 3506−3520.
20. Kocic, N.; Blank, D.; Abufager, P.; Lorente, N.; Decurtins, S.; Liu, S.-X.; Repp, J. Implementing functionality in molecular self-assembled monolayers. *Nano Lett.* **2019**, *19*, 2750−2757.
21. Ramazanoglu, M.; W Ratcliff, I.; Choi, Y.; Lee, S.; Cheong, S.-W.; Kiryukhin, V. Temperature-dependent properties of the magnetic order in single-crystal $BiFeO_3$. *Phys. Rev. B* **2011**, *83*, 174434.
22. Nagarajan, V.; Roytburd, A.; Stanishevsky, A.; Prasertchoung, S.; Zhao, T.; Chen, L.-Q.; Melngailis, J.; Auciello, O.; Ramesh, R. Dynamics of ferroelastic domains in ferroelectric thin films. *Nat. Mater.* **2003**, *2*, 43−47.

23. Qiu, C.; Wang, B.; Zhang, N.; Zhang, S.; Liu, J.; Walker, D.; Wang, Y.; Tian, H.; Shrout, T. R.; Xu, Z. Transparent ferroelectric crystals with ultrahigh piezoelectricity. *Nature* **2020**, *577*, 350−354.

24. Keen, D. A.; Goodwin, A. L. The crystallography of correlated disorder. *Nature* **2015**, *521*, 303−309.

25. Simonov, A.; Goodwin, A. L. Designing disorder into crystalline materials. *Nat. Rev. Chem.* **2020**, *4*, 657−673.

26. Kamiya, K.; Takeuchi, T.; Kabeya, N.; Wada, N.; Ishimasa, T.; Ochiai, A.; Deguchi, K.; Imura, K.; Sato, N. Discovery of superconductivity in quasicrystal. *Nat. Commun.* **2018**, *9*, 154.

27. Tsai, A.-P.; Guo, J.; Abe, E.; Takakura, H.; Sato, T. J. A Stable binary quasicrystal. *Nature* **2000**, *408*, 537−538.

28. Paßens, M.; Caciuc, V.; Atodiresei, N.; Feuerbacher, M.; Moors, M.; Dunin-Borkowski, R. E.; Blügel, S.; Waser, R.; Karthäuser, S. Interface-driven formation of a two-dimensional dodecagonal fullerene quasicrystal. *Nat. Commun*. **2017**, 8, 15367.

29. Wasio, N. A.; Quardokus, R. C.; Forrest, R. P.; Lent, C. S.; Corcelli, S. A.; Christie, J. A.; Henderson, K. W.; Kandel, S. A. Self-assembly of hydrogen-bonded two-dimensional quasicrystals. *Nature* **2014**, 507, 86−89.

30. Overy, A. R.; Cairns, A. B.; Cliffe, M. J.; Simonov, A.; Tucker, M. G.; Goodwin, A. L. Design of crystal-like aperiodic solids with selective disorder–phonon coupling. *Nat. Commun.* **2016**, *7*, 10445.

31. Bauert, T.; Merz, L.; Bandera, D.; Parschau, M.; Siegel, J. S.; Ernst, K.-H. Building 2D crystals from 5-fold-symmetric molecules. *J. Am. Chem. Soc.* **2009**, 131, 3460−3461.

32. Cui, D.; Ebrahimi, M.; Macleod, J. M.; Rosei, F. Template-driven dense packing of pentagonal molecules in monolayer films. *Nano Lett.* **2018**, 18, 7570–7575.

33. Karan, S.; Wang, Y.; Robles, R.; Lorente, N.; Berndt, R. Surface-supported supramolecular pentamers. *J. Am. Chem. Soc*. **2013**, 135, 14004–14007.

34. Vives, G.; Rapenne, G. Directed synthesis of symmetric and dissymmetric molecular motors built around a ruthenium cyclopentadienyl tris(indazolyl)borate complex. *Tetrahedron* **2008**, *64*, 11462−11468.

35. Asato, R.; Martin, C. J.; Gisbert, Y.; Abid, S.; Kawai, T.; Kammerer, C.; Rapenne, G. Ruthenium complexes of sterically-hindered pentaarylcyclopentadienyl ligands. *RSC Advances* **2021**, *11*, 20207−20215.

36. Yeung, K. H. A.; Kühne, T.; Eisenhut, F.; Kleinwächter, M.; Gisbert, Y.; Robles, R.; Lorente, N.; Cuniberti, G.; Joachim, C.; Rapenne, G.; Kammerer, C.; Moresco, F. Transmitting stepwise rotation among three molecule-gear on the Au(111) surface. *J. Phys. Chem. Lett.* **2020**, *11*, 6892−6899.

37. Saywell, A.; Greń, W.; Franc, G.; Gourdon, A.; Bouju, X.; Grill, L. Manipulating the conformation of single organometallic chains on Au(111). *J. Phys. Chem. C* **2014**, *118*, 1719−1728.

38. de Oteyza, D. G.; Silanes, I.; Ruiz-Osés, M.; Barrena, E.; Doyle, B. P.; Arnau, A.; Dosch, H.; Wakayama, Y.; Enrique Ortega, J. Balancing intermolecular and molecule–substrate interactions in supramolecular assemblies. *Adv. Funct. Mater.* **2009**, *19*, 259−264.

39. Kawai, S.; Sadeghi, A.; Xu, F.; Peng, L.; Orita, A.; Otera, J.; Goedecker, S.; Meyer, E. Extended halogen bonding between fluorinated aromatic molecules. *ACS Nano* **2015**, *9*, 2574−2583.

40. Scudiero, L; Hipps, K. W.; Barlow D. E. A self-organized two-dimensional bimolecular structure. *J. Phys. Chem. B* **2003**, *107*, 2903-2909.

41. Gao, H.; Sekutor, M.; Liu. L.; Timmer. A.; Schreyer. H.; Mönig. H.; Amirjalayer. S.; Fokina. N. A.; Studer. A.; Schreiner. P. R.; Fuchs. H. Diamantane suspended single copper atoms. *J. Am. Chem. Soc.* **2018**, *141*, 315-322.
42. Data, N. Numerical data and functional relationships in science and technology. Berlin: Springer, **2009**.
43. Perdew, J. P.; Burke, K.; Ernzerhof, M. Generalized Gradient Approximation Made Simple. *Phys. Rev. Lett.* **1996**, *77*, 3865-3868.
44. Grimme, S.; Antony, J.; Ehrlich, S.; Krieg, H. A Consistent and Accurate Ab Initio Parametrization of Density Functional Dispersion Correction (DFT-D) for the 94 Elements H-Pu. *J. Chem. Phys.* **2010**, *132*, 154104.
45. Goedecker, S.; Teter, M.; Hutter, J. Separable dual-space Gaussian pseudopotentials. *Phys. Rev. B* **1996**, *54*, 1703-1710.
46. Kühne, T. D.; Iannuzzi, M.; Del Ben, M.; Rybkin, V. V.; Seewald, P.; Stein, F.; Laino, T.; Khaliullin, R. Z.; Schütt, O.; Schiffmann, F.; et al. CP2K: An electronic structure and molecular dynamics software package-Quickstep: Efficient and accurate electronic structure calculations. *J. Chem. Phys.* **2020**, *152*, 194103.
47. Momma, K.; Izumi, F. VESTA3 for three-dimensional visualization of crystal, volumetric and morphology data, *J. Appl. Cryst.* **2011**, *44*, 1272-1276.
48. Lu, T.; Chen, F. Multiwfn: A multifunctional wavefunction analyzer. *J. Comput. Chem.* **2012**, *33*, 580-592.

Supplementary Informations

I. Experimental section

I.1. General synthetic methods

All commercially available chemicals were of reagent grade and were used without further purification. Acetic acid, chloroform, sodium chloride, sodium hydroxide, sodium sulfate, sodium hydrogenocarbonate, were purchased from FUJIFILM Wako Pure Chemical Corporation. Ammonium chloride, dichloromethane, ethylacetate, were purchased from Nacalaitesque. 3-Bromofluorobenzene, 3-bromotoluene, hydrogen bromide (30% in acetic acid), *n*-buthyllithium (ca. 15% in hexane) and tetraphenylcyclopentadienone (**2**) were purchased from TCI. Column chromatography was carried out on Wakosil® 60. Thin layer chromatography (TLC) was performed on TLC silica gel 60 F254 plates (Merck) with visualization by using ultraviolet irradiation (λ = 254, 365 nm). ^{1}H and ^{13}C NMR spectra were recorded on JEOL FT-NMR JNM-ECX400P and JEOL FT-NMR JNM-ECX500 spectrometers. Residual solvent signals were used as internal reference for ^{1}H and ^{13}C NMR. Chemical shifts (δ) are reported in ppm. Coupling constants (J) are given in Hz and the following abbreviations have been used to describe the signals: singlet (s); broad singlet (br. s); doublet (d); triplet (t); quadruplet (q); quintuplet (quint); multiplet (m). High-resolution mass spectra (HRMS) were performed with a Waters GCT Premier spectrometer for desorption chemical ionization (DCI/CH_4), with a Waters Xevo G2 QTOF spectrometer for electrospray ionization (ESI), and with a Waters MALDI micro MX spectrometer for matrix-assisted laser desorption ionization (MALDI) (matrix: *trans*-2-[3-(4-*tert*-butylphenyl)-2-methyl-2-propenylidene]malono-nitrile DTCB).

I.2. Synthesis of the compounds

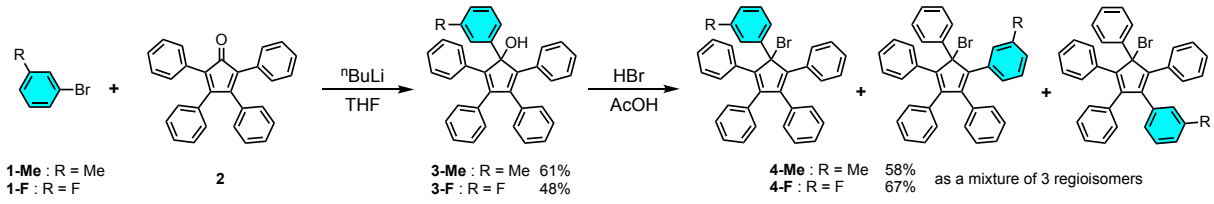

a. 2,3,4,5-Tetraphenyl-1-(*m*-tolyl) cyclopenta-2,4-dien-1-ol (3-Me):

In a flame dried two-necked round bottom flask equipped with a stir bar, 3-bromotoluene **1-Me** (383 µl, 3 mmol, 1.5 eq.) was added under N_2 at RT. Anhydrous THF (7.5 ml) was added and cooled down to -78°C and then, a 1.6 M solution of *n*-buthyllithium in *n*-hexane (1.3 ml, 2 mmol, 1 eq.) was added dropwise. The suspension was stirred for 30 minutes at -78 °C and a degassed solution of 2,3,4,5-tetraphenylcyclopenta-2,4-dienone **2** (769 mg, 2 mmol, 1 eq.) in anhydrous THF (23 ml) was added dropwise. The reaction was stirred 2h at -78°C before being neutralized by a saturated NH_4Cl aqueous solution (ca. 30 ml). After extraction with Et_2O, the combined organic phase was washed three times with water and once with brine. The organic solution was dried over Na_2SO_4, filtered and evaporated. The crude product was purified by silica gel column chromatography using *n*-hexane/CH_2Cl_2 (5/2 to 2/1) as eluant to afford **3-Me** (590 mg, 61%). ^{1}H NMR ($CDCl_3$, 400 MHz, 293 K) δ (ppm): 7.33-7.19 (m, 2H), 6.85-7.10 (m, 7H), 6.96-7.06 (m, 14H), 2.43 (s, 1H), 2.27 (s, 3H, CH_3); ^{13}C NMR ($CDCl_3$, 100 MHz, 293 K) δ (ppm): 148.0, 142.5, 140.1, 135.2, 134.0, 131.2, 130.0, 129.6, 128.6, 128.4, 127.8, 127.1, 127.0, 122.2, 21.9(CH_3); HR-MS (positive, ESI): Calcd for $[C_{36}H_{28}O]^+$: 476.2140 Found: 476.2138

b. [5-Bromo-1,2,3,4-tetraphenyl-5-(*m*-tolyl)]-cyclopenta-1,3-diene (4-Me)

3-Me (80 mg, 0.17 mmol, 1 eq.) and AcOH (3.1 ml) was added to the two-necked round bottom flask equipped with a stir bar and a reflux condenser. After heating to 60°C, 30 % HBr in AcOH (860 µl, 64%) was added dropwise. After cooling down to RT, water was added and the solution was neutralized with aqueous Na_2CO_3. The precipitate was filtered out and washed with water. The crude product was purified by silica gel column chromatography using *n*-hexane/CH_2Cl_2(5/1) as eluant to afford **4-Me** as a yellow solid composed of a mixture of three regioisomers in a 1:1.5:1.5 ratio (53 mg, 58%). ^{1}H NMR ($CDCl_3$, 400 MHz, 293 K) δ (ppm): 7.46-7.49 (m, 7H), 7.22-7.25 (m, 10H), 6.88-7.16 (m, 82H), 6.71-6.77 (m, 7H), 2.26 (s, 3H, CH_3), 2.10 (s, 5.0H, CH_3), 2.06 (s, 4.5H, CH_3); ^{13}C NMR ($CDCl_3$, 100 MHz, 293 K) δ (ppm): 148.5, 148.4, 148.3, 148.2, 148.0, 142.0, 142.0, 141.8, 141.7, 138.0, 137.3, 137.0, 136.8, 136.0, 135.7, 135.6, 134.9, 134.8, 134.6, 134.3, 134.0, 131.2, 130.9, 130.6, 130.5, 130.5, 130.2, 128.0, 127.9, 127.9, 127.8, 127.8, 127.8, 127.7, 127.6, 127.6, 127.5, 127.5, 127.3, 127.3, 127.2, 127.2, 124.3, 21.6, 21.5, 21.4; HR-MS (MALDI-TOF, positive, DCTB): Calcd. for $[C_{36}H_{27}Br]^+$: 538.1296, Found: 538.1307.

c. 1-(*m*-Fluorophenyl)-2,3,4,5-tetraphenylcyclopenta-2,4-dien-1-ol (3-F):

In a flame dried two-necked round bottom flask equipped with a stir bar, 1-bromo-3-fluorobenzene **1-F** (220 µl, 2 mmol, 1.5 eq.) was added under N_2 at RT. Anhydrous THF (5 ml) was added and cooled down to -78°C and then, a 1.6 M solution of *n*-buthyllithium in *n*-hexane (1.7 ml, 2.7 mmol, 2 eq.) was added dropwise. The suspension was stirred for 30 minutes at this temperature and a degassed solution of 2,3,4,5-tetraphenylcyclopenta-2,4-dienone **2** (525 mg, 1.33 mmol, 1eq.) in anhydrous THF (23 ml) was added dropwise. The reaction was stirred 2h at -78°C before being neutralized by pouring a saturated NH_4Cl aqueous solution (ca. 20 ml). After extraction with Et_2O, the combined organic phase was washed three times with water and once with brine. The organic solution was dried over Na_2SO_4, filtered and evaporated. The crude product was purified by silica gel column chromatography using *n*-hexane/CH_2Cl_2 (5/2 to 2/1) as the eluant to afford **3-F** (316 mg, 48%). ^{1}H NMR (MeOD-d^4, 500 MHz, 293 K) δ (ppm): 7.36 (d, J= 8 Hz, 1H), 7.22-7.28 (m, 2H), 7.09-7.15 (m, 6H), 6.93-7.04 (m, 14H), 6.85 (dt, J= 2.5 and 8.4 Hz, 1H); ^{13}C NMR ($CDCl_3$, 100 MHz, 293 K) δ (ppm): 164.3, 161.9, 147.5, 143.4, 143.3, 142.8, 134.8, 133.5, 130.0, 129.9, 129.9, 129.4, 127.9, 127.8, 127.2, 127.8, 127.2, 127.2, 120.7, 120.6, 114.0, 113.8, 112.5, 112.2, 89.7; ^{19}F NMR ($CDCl_3$, 400 MHz, 293 K) δ (ppm): −122.69 (s, 1F); HR-MS (positive, ESI): Calcd for $[C_{35}H_{26}FO]^+$: 481.1962 Found: 481.1967.

d. [5-Bromo-1,2,3,4-tetraphenyl-5-(*m*-fluorophenyl)]-cyclopenta-1,3-diene (4-F)

3-F (127 mg, 0.26 mmol, 1 eq.) and AcOH (4.5 ml) was added to the two-necked round bottom flask equipped with a stir bar and a reflux condenser. After heating to 60°C, 30% HBr in AcOH (1.3 ml, 26 eq.) was added dropwise and stirred for 45 min. After cooling down to RT, water was added and the solution was neutralized with an aqueous solution of Na_2CO_3. The precipitate was filtered and washed with water. The crude product was purified by silica gel column chromatography using *n*-hexane/CH_2Cl_2(6/1) as eluant to afford **4-F** (97 mg, 67%) as a yellow solid composed of a mixture of regioisomers in a 1:2.5:3 ratio. ^{1}H NMR ($CDCl_3$, 500 MHz, 293 K) δ (ppm): 7.45-7.48 (m,10H), 7.23-7.25 (m, 7H), 7.02-7.19 (m, 59H), 6.92-7.00 (m, 39H), 6.83 (ddt, J=0.8, 2.7, 8.6 Hz, 2H), 6.78 (ddt, J=0.8, 2.7, 8.6 HZ, 2H), 6.70-6.75 (m, 7H), 6.66 (qd, J=1.5, 2.4, 9.9 Hz, 2H).

^{13}C NMR ($CDCl_3$, 100 MHz, 293 K) δ (ppm): 163.9, 163.4, 163.1, 161.5, 160.9, 160.7, 149.3, 148.7, 148.2, 147.9, 146.7, 142.7, 142.2, 141.6, 141.4, 140.5, 138.9, 138.8, 136.9, 138.8, 136.9, 136.8, 136.3, 136.2, 135.4, 134.4, 134.4, 134.3, 133.9, 133.8, 133.7, 130.4, 130.3, 130.0, 129.2, 128.8, 128.4, 128.5, 128.4, 128.0, 127.9, 127.7, 127.5, 127.4, 127.4, 127.3, 127.3, 127.2, 127.2,

126.3, 126.3, 125.9, 125.8, 123.0, 117.2, 117.0, 116.8, 115.1, 114.9, 114.7, 114.3, 114.1, 114.1, 113.9; ^{19}F NMR ($CDCl_3$, 376 MHz, 293 K) δ (ppm): −112.45 (m, 1F), −113.40 (m, 2.4F), −113.65 (m, 3.1F); HR-MS (MALDI-TOF, positive, DCTB): Calcd. for $[C_{35}H_{24}BrF]^+$: 542.1045, Found: 542.1063.

II. Additional STM images

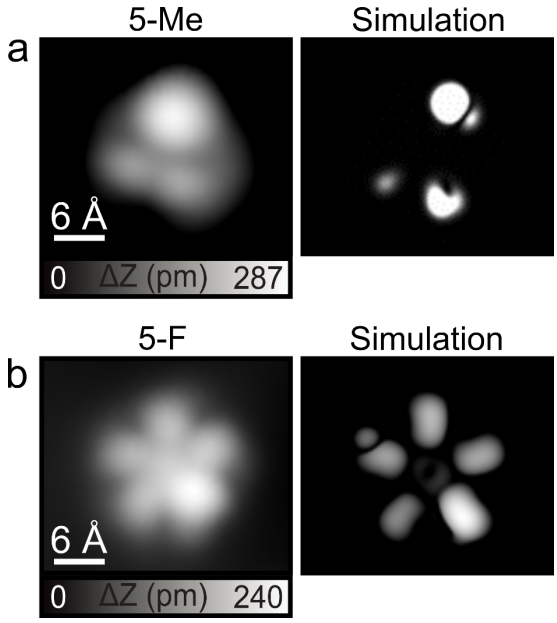

Figure S1. STM images of (a) **5-Me** and (b) **5-F** on the Au(111) surface, along with the corresponding simulated STM images based on their optimized structures.

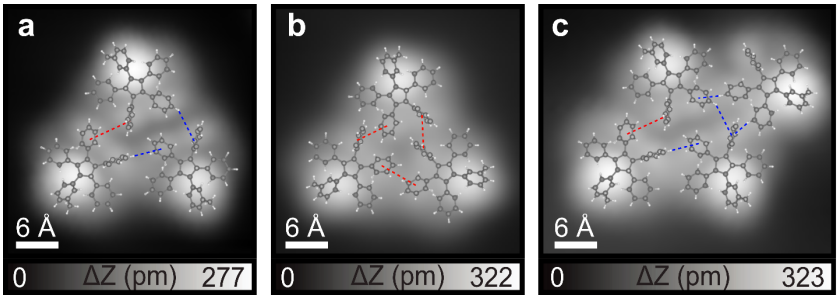

Figure S2. Close-up views of the asymmetric trimer, symmetric trimer, and tetramer with the calculated structural model of **5-Me** superimposed. The π-π interactions and CH-π interactions are depicted by red and blue dashed lines, respectively. Structural model: H: white, C: gray.

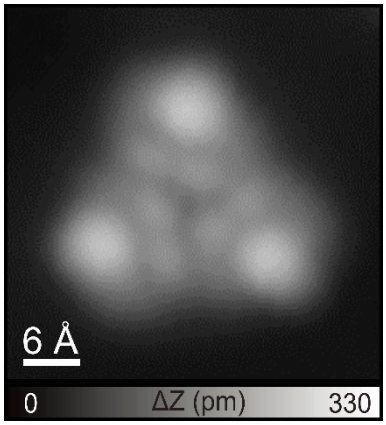

Figure S3. Another chirality of the trimer of **5-Me** on Au(111). Scanning parameter: V = 0.2 V and I = 10 pA.

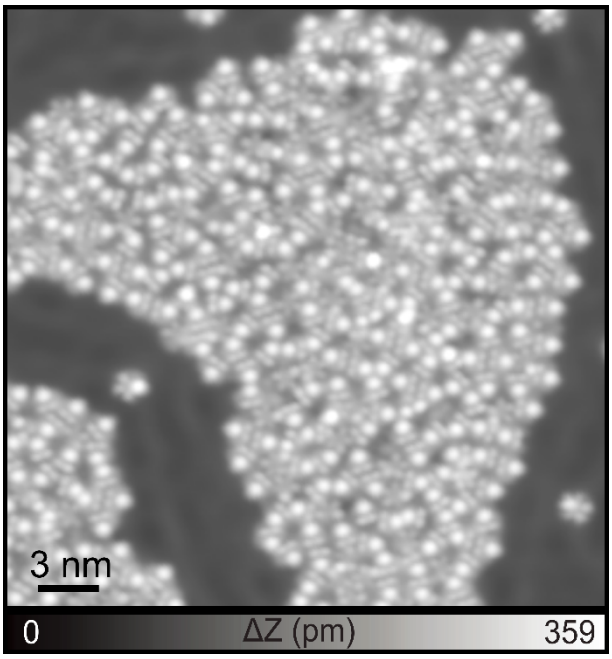

Figure S4. Close-packed island structure of **5-Me** on the Au(111) surface showing the herringbone around the island. Scanning parameter: V = 0.2 V and I = 10 pA.

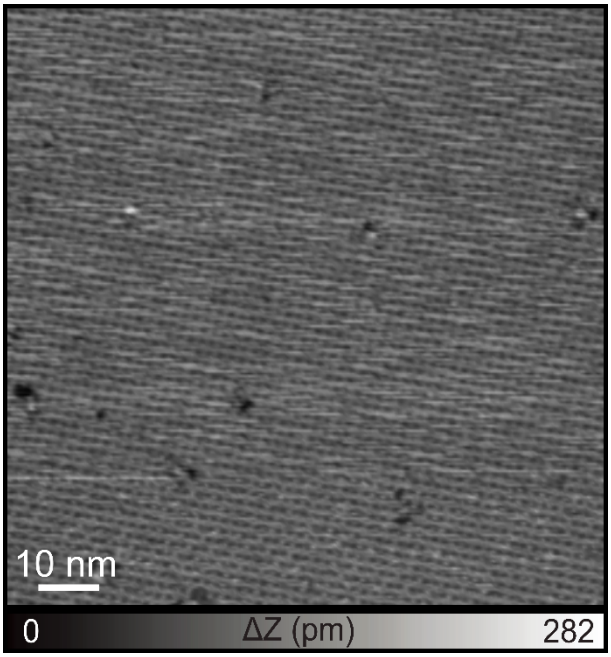

Figure S5. Large-scale STM image of **5-Me** on the Ag(111) surface. Scanning parameter: V = 0.2 V and I = 10 pA.

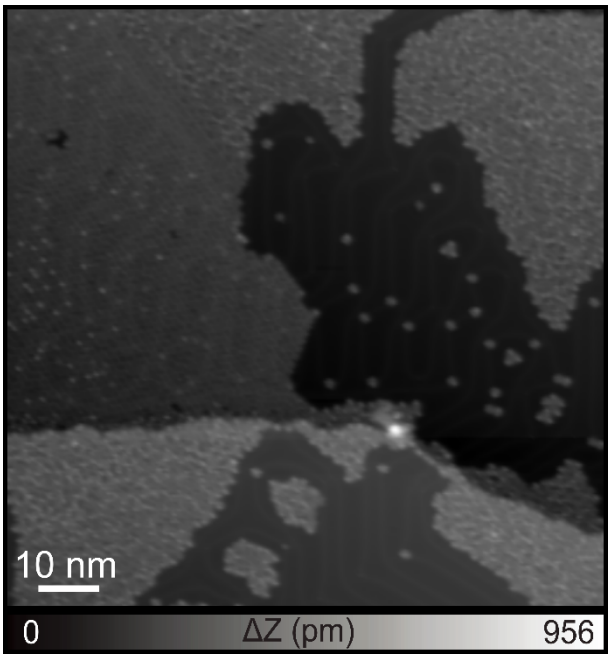

Figure S6. Large-scale STM image of **5-F** on the Au(111) surface. Scanning parameter: V = 0.2 V and I = 10 pA.

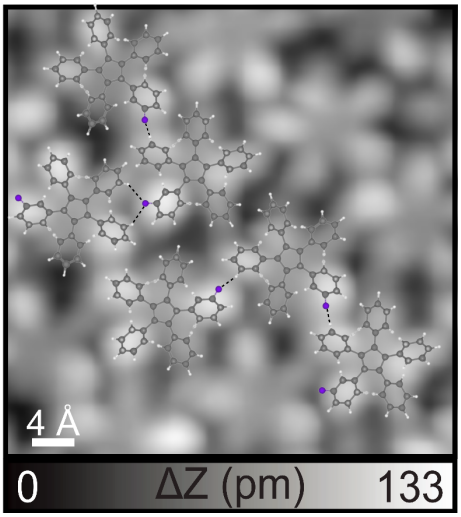

Figure S7. Close-up view of the phase I with the calculated structural model of star-shaped **5-F** superimposed. The CH···F interactions are depicted by black dashed lines. Structural model: H: white, C: gray, F: blue.

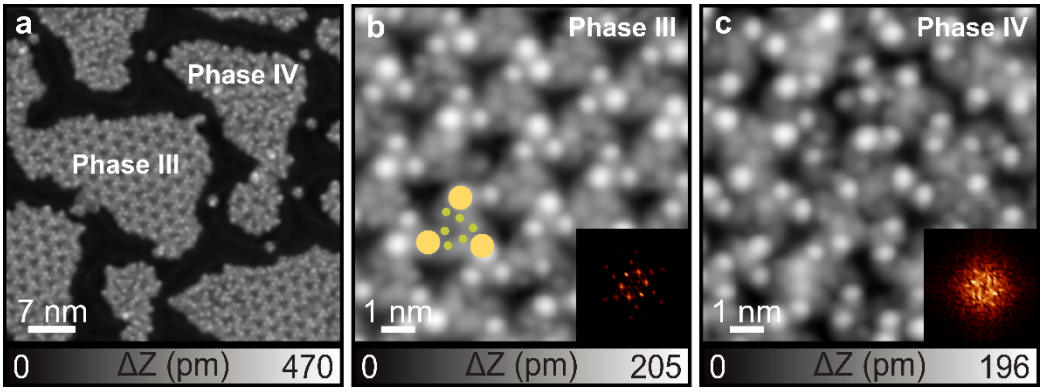

Figure S8. Phase transformation of **5-F** self-assembled structures by annealing at 100 °C on Au(111). (a) Large-scale STM image of the new phases. (b, c) Close-up views of phase III and phase IV, respectively. Insets show corresponding 2D-FFT images. Scanning parameter: V = 0.2 V and I = 10 pA.